CrystEngComm

Accepted Manuscript

ROYAL SOCIETY OF CHEMISTRY

www.rsc.org/crystengcomm

Journal Name

RSCPublishing

ARTICLE

Crystal-to-Crystal Transformation in Solid-State Electrochemical Doping of Cl^- Ions to a Nano-Porous Neutral Radical, Lithium Phthalocyanine; Revelation of Electron-Electron Correlations in a 1D Half-Filled System

Cite this: DOI: 10.1039/xoxxoooooox

Received ooth January 2012,
Accepted ooth January 2012

DOI: 10.1039/xoxxoooooox

www.rsc.org/

Yasuhito Miyoshi,[a] Hirofumi Yoshikawa[a] and Kunio Awaga*[a,b]

We carried out electrochemical doping of Cl^- ions to the x-form single crystals of a neutral π radical LiPc, in which the structure consists of 1D stacking chains of LiPc and nano-channels parallel to them. It was found that the LiPc crystals on the working electrode were electrochemically oxidized in an acetonitrile solution of tetrabutyl ammonium chloride (TBA·Cl), exhibiting a crystal-to-crystal transformation to LiPc·Cl_x ($0<x<0.5$), in which the x value was controlled by the electrochemical potential. The crystal structures of the LiPc·Cl_x series were successfully solved and refined by the X-ray single-crystal analysis, and the obtained structures clearly indicated the presence of the Cl^- ions in the 1D channels, and a systematic structural change in the π stacking chain of LiPc. Namely, as the value of x increased, the interplanar distance between the neighboring LiPc molecules showed a decrease, which was associated with a significant enhancement of the conductivity. These oxidative-doping effects indicate that the structural and electrical properties of the 1D half-filled electron system of LiPc are governed by the electron-electron correlations between the unpaired electrons.

Introduction

Solid-state electrochemistry is a powerful tool to control the valences and properties of materials. In a conventional electrochemical cell, a thin layer of an electroactive material on the working electrode is oxidized/reduced by the potential difference between the working and counter electrodes. This process is associated with doping of counter anions/cations from the electrolyte solution (see Scheme 1). The most significant advantage of this electrochemical doping is a precise and reversible control of the dopant concentration under electrochemical equilibrium, which is tuned by the potential of the working electrode. While this doping technique has been extensively applied to semiconductive organic polymers such as polyacetylene,[1] polythiophene,[2] and polyaniline[3] in order to control their conductivity, color, etc., the application to the solids of small molecules has been limited,[4-7] because these materials are much more soluble into electrolyte solutions than organic polymers, especially after electrochemical oxidation/reduction. The limited examples include macrocycles such as phthalocyanines (abbreviated as Pc), because they form robust thin films against the redox cycles due to their strong intermolecular interactions.

LiPc (see Scheme 1) is a well-known neutral π radical,[8] while the other divalent MPcs have a closed-shell π system. The crystals of LiPc exhibit three polymorphs: monoclinic α- and β-forms and a tetragonal x-form. While the structures of the α- and β-forms are common to those for the divalent MPcs, the x-form is unique to the π-radical Pcs, such as LiPc,[9] NiPc·I[10] and FePc·X.[11] This structure consists of 1D uniform π-stacking chains with a large face-to-face overlap that is much larger than those in the α- and β-forms,[12] and between the 1D chains of LiPc, there are 1D cavities parallel to the chains, and these cavities are large enough to accommodate small gas molecules such as N_2 and O_2. It is known that the EPR linewidth of x-LiPc is significantly dependent on the concentration of O_2, and thus this compound is applicable to O_2 sensors.[13] Due to the presence of the unpaired electron, LiPc exhibits electrical and magnetic properties[14-16]; e.g., the resistivity of the single crystals of LiPc (10^3 Ω cm) is much lower than those of the other Pc crystals (~ 10^7 Ω cm).[17] The polarized reflectance measurements indicated that LiPc can be characterized as a Mott-Hubbart system with a transfer integral t and an effective Coulomb energy $U_{eff} = U - V$, where U and V are on-site and inter-site Coulomb energies, respectively.[18]

Recently, we examined the solid-state electrochemistry of the crystalline thin-films of LiPc, which were prepared by vacuum deposition. The as-prepared films in the α-form exhibit irreversible structural transformation to the x-form after the electrochemical oxidation to LiPc·X (X= BF_4^-, ClO_4^-). Then,

the obtained x-form thin films exhibit a reversible electrochemical doping/dedoping of X, maintaining the structure of the x-form.[19] This structural persistence of the x-form under the electrochemical redox cycles is probably caused by its nano-porous structure. Note that the crystalline thin-films of ZnPc in the α-form become amorphous after the electrochemical doping of counter ions.[20]

The structural and electrochemical features of the x-form LiPc inspired us to examine the solid-state electrochemistry of its single crystals. In the present work, we carried out the electrochemical doping of Cl^- into the x-form single crystals of LiPc, and found a crystal-to-crystal transformation from LiPc to LiPc·Cl_x. We report the crystal structures and the electrical properties of the LiPc·Cl_x series, which are significantly dependent on the doping level, x.

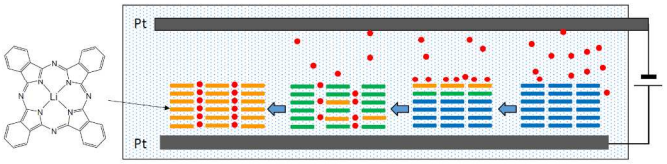

Scheme 1 Solid-sate electrochemical doping of ions to the x-form LiPc thin-film/crystal. Red circles represent the counter ions. Blue, green, and orange rectangles represent the LiPc molecules in different oxidative states.

Experimental

Preparation of LiPc Crystals

LiPc crystals were grown by the electrochemical oxidation of Li_2Pc under a constant current condition, using an H-shaped glass that consisted of the anode and cathode compartments (see Scheme 2(a)). They were separated by a glass filter (pore size: 40–50 μm) for a slow diffusion speed. The electrodes were platinum rods with a diameter of 1 mm, and the supporting electrolyte was tetrabutylammonium perchlorate (TBA·P). TBA·P was purified by recrystallization from a mixed solution of ethyl acetate and toluene prior to use, and dried under a vacuum for at least one day. To each compartment were added 100 mg of TBA·P and 8 mL of acetonitrile, and 20 mg of Li_2Pc prepared by a method described in the literature[21] was added to the anode side. This electrochemical cell was set under a nitrogen atmosphere, to prevent contaminations of water and oxygen from the air. After dissolving all reagents, the electrolysis was started using a constant current regulator (YAZAWA CS-12Z). Within 3–4 weeks, dark-green needle-shaped crystals of LiPc of 0.2–1.0 mm in length were grown on the surface of the platinum anode. Keeping the crystals on the electrode, we washed them with acetonitrile three times, and then dried them in air.

Electrochemical Doping of Cl^- Ions to LiPc Crystals

The electrochemical doping of Cl^- ions to the LiPc crystals was carried out using a three-electrode electrochemical cell that contained a 0.1 mol dm^{-3} tetrabutyl ammonium chloride (TBA·Cl)/acetonitrile solution, as shown in Scheme 2(b). The platinum electrode on which the LiPc crystals were grown was used as a working electrode. An Ag/Ag^+ electrode (BAS Co., Ltd.) and a platinum electrode (1 mm in diameter) were used as reference and counter electrodes, respectively. A constant potential was loaded on the working electrode under a nitrogen atmosphere, using a Hokuto Denko HZ-5000 electrochemical analyzer. We stopped doping, when the doping current became constant (see Fig. 2).

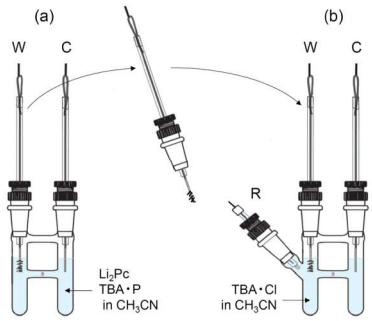

Scheme 2 (a) Electrochemical crystal growth of LiPc and (b) electrochemical doping of Cl^- ions to the single crystals of LiPc.

Single-Crystal X-ray Structural Analysis

XRD data for the obtained crystals of LiPc·Cl_x were collected at 173 K on a Rigaku RA-Micro7 equipped with a Saturn70 CCD detector, using graphite-monochromated Mo K_α (λ=0.71073 Å) radiation. The crystal structures were solved by a direct method using the SHELXS-97 program[22] and refined by successive differential Fourier syntheses and a full-matrix least-squares procedure using the SHELXL-97 program.[23] The occupancy of the Cl^- ions in LiPc·Cl_x was first optimized, assuming isotropic thermal ellipsoids for these ions. Then, fixing the occupation number, all non-hydrogen atoms including Cl^- were anisotropically refined. Hydrogen atoms were located by the differential Fourier synthesis and were isotropically refined.

Physical Measurements

Cyclic voltammograms (CVs) were measured on a Hokuto Denko HZ-5000 electrochemical analyzer. Scanning electron microscopy (SEM) images and energy dispersive X-ray (EDX) spectra were obtained using a Hitachi S-4300 field-emission SEM equipped with a Horiba EMAX 6853-H EDS system. Conductivity measurements were performed by a two-probe method under a vacuum and the sample temperature was monitored by a thermocouple. EPR measurements were performed on a JEOL JES-FA200.

Results and Discussion

CV of LiPc Crystals

The x-form LiPc single-crystals were grown by the electrochemical oxidation of Li_2Pc in an acetonitrile solution of TBA·P. Then the Pt electrode on which the LiPc crystals had been grown was transferred to a three-electrode electrochemical cell, and was used as a working electrode for the CV measurements and the electrochemical doping (see Scheme 2).

To investigate the oxidation potential of the LiPc crystals, the CV measurements were performed in a 0.1 mol dm^{-3} acetonitrile solution of TBA·Cl. The results are shown in Fig. 1, where panel (a) shows the data at the scan rate of 1 mV/s, and panel (b) shows the scan rate dependence of the CV curves from 0.2 to 500 mV/s. The curve at 1 mV/s clearly indicates the

anodic and cathodic peaks at 0.4 and 0.3 V, respectively. This confirms the electrochemical oxidation and re-reduction of LiPc even in its crystals. These processes are associated with the penetration and detachment of the counter ion, Cl^-, respectively, as shown later. As the scan rate increases, the two peaks exhibit an enhancement in intensity and the CV curves become less symmetric. In addition, the oxidation and re-reduction peaks exhibit significant high- and low-voltage shifts, respectively. This is more obvious for the re-reduction peaks, as indicated by the arrow in Fig. 1(b). At the high scan rates, the CV curves become much less symmetric, with an increase in the potential difference between the anodic and cathodic peaks. In general, the reversibility between the oxidation and re-reduction processes on the CV curves is governed by the diffusion rate of the reactants (redox species). In the present case, however, the reactant, LiPc, is fixed on the working electrode, so that the reaction kinetics is not governed by the reactant diffusions, but by the diffusion of the counter anion, Cl^-, in the crystals of LiPc.[24-26] Therefore, the irreversible behavior of the CV curves at the high scan rates indicates a slow diffusion of the counter anions. In contrast, the voltage difference between the anodic and cathodic peaks is as small as *ca*. 80 mV when the scan rate is less than 1 mV s^{-1}. This value of the voltage difference roughly agrees with the theoretical one of 57 mV at room temperature for the reversible systems, which is estimated based on the fact that the redox peak potential is shifted by 28.5 mV from the half wave potential in the one-electron redox reaction.[27] As a result, the CV curves at the slow scan rates (< 1 mVs^{-1}) are quasi-reversible, indicating that the motion of the Cl^- ions is smooth in the lattice of LiPc.

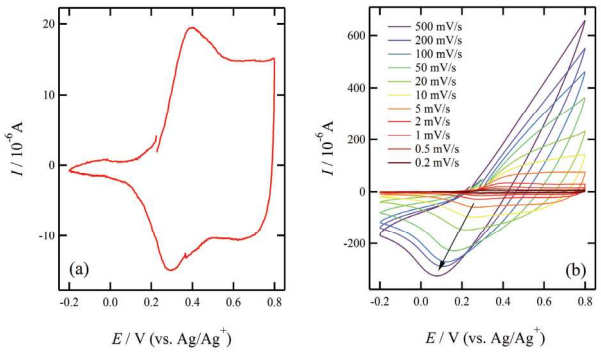

Fig. 1 (a) Cyclic voltammogram of LiPc crystals in 0.1 mol dm^{-3} acetonitrile solution of tetrabutylammonium chloride, measured at 1 mV/s , and (b) those at various scan rates from 0.2 to 500 mV/s. The arrow in (b) indicates a shift of the re-reduction peaks, dependent on the scan rates.

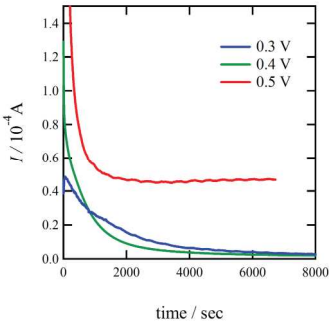

Fig. 2 Time trajectory of the oxidation current in the electrochemical doping at 0.3, 0.4, and 0.5 V.

Since the oxidation was found around 0.4 V in the scan rate of 1.0 mV/s (see Fig. 1(a)), we measured the time evolution of the oxidation current due to the electrochemical doping at the constant voltages of 0.3, 0.4 and 0.5 V. The results are shown in Fig. 2. The time dependences of the oxidation current at 0.3 (blue) and 0.4 V (green) are similar; the current shows a quick decrease with an insertion of the Cl^- ions into the crystals, and becomes nearly zero after complete doping within several hours. It is notable that this completing time exhibited a significant sample dependence. In contrast, the electrolysis curve (red) at 0.5 V is quite different from the others. The current decreases at the beginning, but reaches at a non-zero value after 2000 sec. In a control experiment using bare platinum electrodes, it was confirmed that the acetonitrile solution of TBA·Cl at 0.1 mol dm^{-3} is oxidized continuously above 0.5 V vs. Ag/Ag^+. Therefore, the non-zero steady-state current at 0.5 V would be caused by the electrochemical oxidation of the Cl^- ions. This means that the electrochemical doping to the LiPc crystals in the TBA·Cl electrolyte should preferably be done in the voltage range less than 0.5 V.

Structural Characterization of LiPc·Cl_x

The electrochemical doping to the LiPc crystals was done at 0.3, 0.4 and 0.5 V. The EDX analyses were performed on the obtained materials—after rinsing with acetonitrile three times to remove the excess electrolyte remaining on the crystal surfaces—in order to determine whether these materials contained Cl^- ions. Figure 3 shows an SEM image of an LiPc·Cl_x crystal, which was doped at 0.3 V. The EDX analysis indicates the presence of Cl and all the elements in LiPc, except hydrogen and lithium atoms due to their small electron densities. We confirmed that the presence of Cl was not caused by the contamination from the electrolyte (TBA·Cl); there was no EDX signal of Cl from the LiPc crystals, which had just been soaked in a TBA·Cl solution of acetonitrile and then rinsed with this solvent prior to EDX measurements. Figure 3 also shows the results of the EDX mapping analysis at the five spots indicated by the yellow circles. The concentration of Cl was calculated from the atomic ratio between Cl and N from the EDX measurements. As indicated in this figure, the Cl concentrations obtained from these spots vary from 0.25 to 0.33. These deviations are within the experimental error of the EDX measurements, namely *ca*. ± 0.1. It is concluded that the fluctuation of the Cl^- concentration in a single LiPc·Cl_x crystal is not very significant.

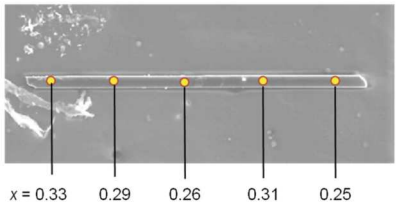

Fig. 3 SEM image of a typical LiPc single crystal prepared at 0.3 V. The values of x indicate the special distribution of the Cl concentrations in LiPc·Cl_x at the five points on the crystal, estimated from the EDX mapping analysis.

We used EDX measurements to examine the Cl concentrations in the numerous LiPc·Cl_x crystals grown at the voltages of 0.3, 0.4 and 0.5 V. Figure 4 shows the variations in *x* for the LiPc·Cl_x crystals grown at the three doping potentials. In this figure, one plot represents the data obtained from one piece of crystal, and the plots at one potential come from the

different crystals grown in the same batch, namely, on the same electrode. The results indicated that, although the fluctuation in x was small in one crystal (see Fig. 3), the value of x changed significantly from crystal to crystal. The obtained x values were 0.34 ± 0.06, 0.43 ± 0.14, and 0.48 ± 0.05 at 0.3, 0.4, and 0.5 V, respectively. This large variation in x would be caused by an inhomogeneity in the effective potential at each crystal, because the conductivity of the LiPc crystals is not very high. Even so, the results in Fig. 4 clearly show that the doping concentration tended to increase with an increase in the potential applied to the working electrode. It is also notable that the dopant concentration x was limited to less than 0.6 at the doping potential of less than 0.5 V.

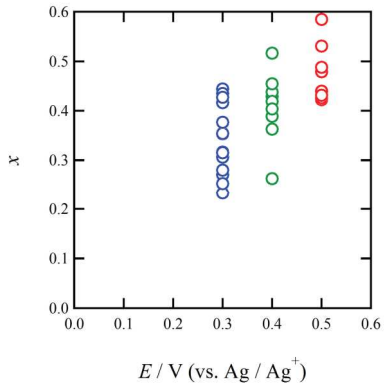

Fig. 4 Concentrations of Cl^- in LiPc·Cl_x at the three doping potentials, obtained by the EDX measurements.

Table 1 Crystallographic data for the selected LiPcClx crystals with various dopant concentrations as well as the pristine x-form LiPc.

Compound	x-LiPc	$LiPcCl_{0.11}$	$LiPcCl_{0.20}$	$LiPcCl_{0.21}$	$LiPcCl_{0.24}$	$LiPcCl_{0.38}$	$LiPcCl_{0.46}$
Crystal system	tetragonal	tetragonal	tetragonal	tetragonal	tetragonal	tetragonal	tetragonal
Space group	*P4/mcc*	*P4/mcc*	*P4/mcc*	*P4/mcc*	*P4/mcc*	*P4/mcc*	*P4/mcc*
a (Å)	13.852(4)	13.8430(9)	13.829(5)	13.864(6)	13.841(4)	13.843(4)	13.8605(7)
c (Å)	6.4216(17)	6.4156(6)	6.406(2)	6.414(3)	6.4027(18)	6.394(2)	6.3917(5)
Volume (Å^3)	1232.2(6)	1229.41(16)	1225.1(7)	1232.8(9)	1226.6(6)	1225.3(6)	1227.93(16)
Z	2	2	2	2	2	2	2

Crystal Structures of LiPc·Cl_x

To obtain information on the crystallinity and structure after the electrochemical doping, we carried out X-ray single-crystal structure analysis on the various LiPc·Cl_x crystals that had been electrochemically doped at 0.3, 0.4, and 0.5 V. Table 1 summarizes the crystallographic data for representative crystals.[28] To our surprise, the crystallinity was well retained and the structures were successfully solved and refined, with a more accurate optimization of the dopant concentration x than that in the EDX measurements. In fact, the value of x changed from crystal to crystal, in the range of $0.1 < x < 0.5$. This agrees with the EDX analyses. It was found that the LiPc·Cl_x series crystals are isostructural to the parent x-form LiPc (see Table 1),[9] except that Cl^- ions exist in the 1D channels. The structure of LiPc·Cl_x is also isostructural to as the iodide salts of Pcs such as LiPc·I[21] and NiPc·I.[10] Figure 5 shows the crystal structure of LiPc·$Cl_{0.38}$ (see also Table 1). The Li^+ ion is located at the center of the inner four nitrogen atoms of a planar phthalocyanine molecule. These LiPc molecules are stacked metal-over-metal so that their molecular planes are perpendicular to the c axis and are staggered by ca 39.1°. The interplanar spacing, namely a half-length of the c axis, is 3.1934(5) Å at 173 K, which is shorter than that in the non-doped LiPc crystal (3.2108(9) Å at 173 K). In the 1D channel, the Cl^- ions occupy a space on the c axis, where they bridge the distances between eight LiPc molecules. The thermal ellipsoid of the Cl^- ions is stretched along the c axis to a length 7- to 10-fold greater than that of the ellipsoids in the transverse directions (the a and b axes). This was probably due to the disorder of the Cl^- ions along the c axis. A similar feature has been reported for $\{[Si(Pc)O]X_y\}_n$[29] and $M(Pc)X_y$.[10]

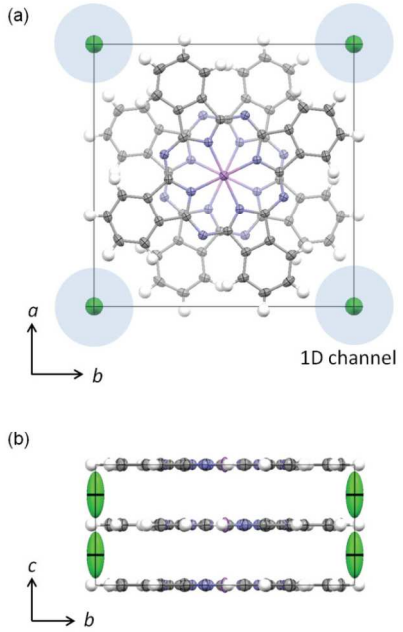

Fig. 5 Crystal structure of LiPc•$Cl_{0.38}$: the projections on the *ab* plane (a) and on the *bc* plane (b). The green ellipses indicate the positions of Li ions.

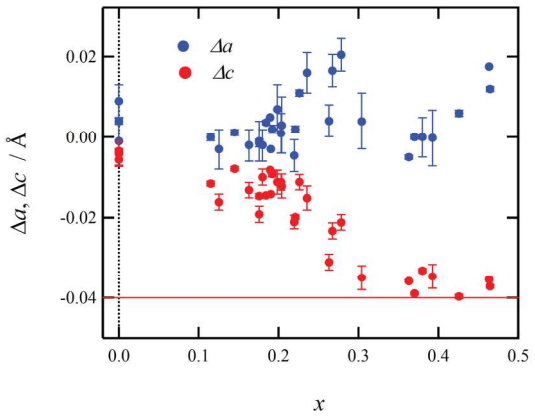

Fig. 6 Dependence of the lattice constants a and c on the Cl^- concentration in LiPc·Cl_x. The red line represents the lattice constant c for LiPc·I.

We have solved the X-ray structures of 32 crystals in the LiPc·Cl_x series. Figure 6 shows the dependence of the lattice constants a and c on the Cl^- concentration x. It is found that the cell parameter a (blue) depends little on x. The Cl^- ions are located in the 1D channels between the LiPc columns, and the ion size (3.34 Å) is smaller than the channel diameter (*ca*. 4 Å).

Therefore, the steric hindrance of the dopant molecules hardly affects the transverse direction of the LiPc molecules, resulting in the little change in the lattice constant *a*. In contrast, the length of the *c* axis (red) decreases significantly with an increase in *x* below 0.3, and becomes constant at values of *x* above 0.3. The initial decrease means a significant decrease in the intermolecular π spacing in the 1D stacking chain of LiPc (see Scheme 3). The red line in Fig. 6 shows the value of the lattice constant *c* (6.38 Å) of LiPc·I, in which the intermolecular distance between the $LiPc^+$ cations is considered to be governed by the electrostatic interactions, namely $LiPc^+•••I^-•••LiPc^+$. The lattice constant *c* of the $LiPc·Cl_x$ series tends to approach this value with an increase in *x*.

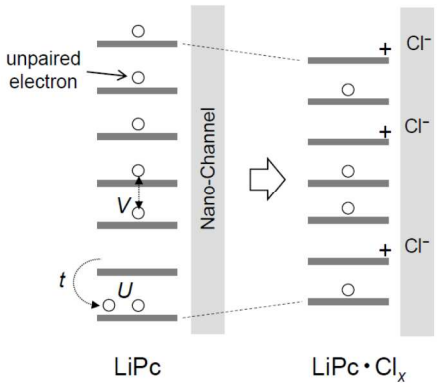

Scheme 3 Effect of the partial removal of the unpaired electrons in the π stacking of the x-form LiPc.

Electrical Conductivity of $LiPc·Cl_x$

The electrical conductivity was measured on the selected $LiPc·Cl_x$ crystals listed in Table 1 using a two-probe technique, along the long axis of the crystal that corresponds to the stacking axis of LiPc molecules (*c* axis).[12] The conductivity measurements were performed under a vacuum in the temperature range between 80-300 K. The sample temperature was monitored by a thermocouple adjacent to the crystal. Figure 7(a) shows the Arrhenius plots for the temperature dependence of the conductivities of the $LiPc·Cl_x$ series with x = 0, 0.11, 0.20, 0.21, 0.24, and 0.38, obtained by the two-probe method. Since the doped LiPc crystals were small and fragile, we could not adopt the four-probe method. All of the crystals exhibit semiconductive properties. The conductivity of the pristine LiPc crystal (x=0) was 7×10^{-3} S cm^{-1} at room temperature, which agrees with the previously reported value.[30] With an increase in *x*, there is a significant enhancement in conductivity, though the removal of the unpaired electrons means a decrease in the carrier density. Figure 7(b) shows the activation energy E_a. The value of E_a (0.14 eV) at x = 0 gradually decreases down to 0.03 eV at x= 0.2. Namely, E_a becomes one-fourth of the original value for the LiPc crystal, due to the electrochemical continuous doping in the same stacking framework of LiPc. However, the decrease in E_a appears to be saturated in the range of $x > 0.2$ before displaying a metallic state. Although it is possible that this saturation is caused by a contact resistance, this observed conductivity enhancement well agrees with the dependence of the lattice constant *c* on *x*, as shown in Fig. 6. This indicates that the decrease in E_a would be caused by the decrease in the intermolecular spacing. It is notable that the room-temperature conductivities of the fully-oxidized $LiPc·I^{31}$ and $NiPc·I^{10}$ (0.2 S cm^{-1}) are similar to that for $LiPc·Cl_x$ with x = 0.2–0.4. The present electrochemical doping of LiPc has revealed the presence of the electron-electron repulsion in the 1D stacking chains of LiPc, which would cause the lower conductivity of the pristine LiPc.

LiPc with a 1D half-filled electron system can be regarded as a Mott insulator, characterized by the three parameters, *t*, *U* and *V*.[18] The conductivity of the neutral LiPc is higher than that of the other divalent MPcs, but still exhibits non-metallic behavior. Since there is no charge ordering in the ground state of LiPc, *U* should be larger than *V*. The electrochemical doping with Cl^- ions means a partial loss of the unpaired electrons in the stacking of LiPc, so that the observed shrinkage along the *c* axis and the conductivity enhancement, would strongly indicate the role of U_{eff} as a structure-controlling factor, and its sensitiveness to the loss of the unpaired electrons.

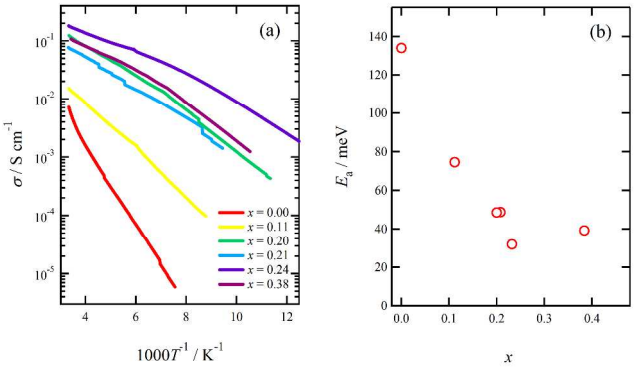

Fig. 7 (a) Temperature dependence of the conductivities of the $LiPc·Cl_x$ crystals. (b) Plots of the composition dependence of the Arrhenius activation energy E_a in $LiPc·Cl_x$.

Conclusions

We carried out electrochemical Cl^- doping to the single crystals of LiPc in the x-form. Due to the presence of nano-porous channels in these crystals, this method realized the crystal-to-crystal transformation to $LiPc·Cl_x$ ($0<x<0.5$), in which the *x* value was controlled by the electrochemical potential of the working electrode. This method is highly applicable to various electroactive materials with nano-porous structures and lattice vacancies, such as MOFs and ionic crystals. The X-ray crystal analyses for $LiPc·Cl_x$ clearly demonstrated the presence of the Cl^- ions in the 1D channels, and the shrinkage of the interplanar distance between the neighboring LiPc molecules. This structural change and the significant enhancement of the conductivity revealed the presence of the strong electron-electron correlation in the parent LiPc with a 1D half-filled electron system.

Acknowledgements

This work was supported by a Grant-in-Aid for Scientific Research from the Ministry of Education, Culture, Sports, Science, and Technology (MEXT). This work was supported by the JSPS Core-to-Core Program, A. Advanced Research Networks.

Notes and References

[a] Department of Chemistry & Research Center for Materials Science, Nagoya University, Chikusa-ku, Nagoya 464-8602, Japan. E-mail: awaga@mbox.chem.nagoya-u.ac.jp; FAX: +81-52-789-2484; Tel: +81-52-789-2487
[b] CREST, Nagoya University, Nagoya 464-8602, Japan.

1 P. J. Nigrey, A. G. MacDiarmid, A. J. Heeger, *J. Chem. Soc., Chem. Commun.,* 1979, 594-595.
2 G. Tourillon, F. Garnier, *J. Electroanal. Chem*., 1984, **161**, 407-414.
3 P. M. McManus, S. C. Yang, R. J. Cushman, *J. Chem. Soc., Chem. Commun.,* 1985, 1556-1557.
4 T. Tominaga, K. Hayashi, N. Toshima, *J. Porphyrins Phthalocyanines*, 1997, **1**, 239-249.
5 T. Maruno, S. Hayashida, K. Sukegawa, *J. Electroanal. Chem*., 1989, **267**, 303-307.
6 J. M. Green, L. R. Faulkner, *J. Am. Chem. Soc.,* 1983, **105**, 2950-2955.
7 Y. Takigawa, R. Watanabe, S. Morita, Y. F. Miura, M. Sugi, *Jpn. J. Appl. Phys.*, 2006, **45**, 394-396.
8 H. Sugimoto, T. Higashi, M. Mori, *J. Chem. Soc., Chem. Commun*., 1983, 622-623.
9 H. Sugimoto, M. Mori, H. Masuda, T. Taga, *J. Chem. Soc., Chem. Commun.* 1986, 962–963.
10 C. J. Schramm, R. P. Scaringe, D. R. Stojakovic, B. M. Hoffman, J. A. Ibers, T. J. Marks, *J. Am. Chem. Soc*., 1980, **102**, 6702-6713.
11 S. M. Palamer, J. L. Stanton, N. K. Jaggi, B. M. Hoffman, J. A. Ibers, L. H. Schwartz, *Inorg. Chem.*, 1985, **24**, 2040-2046.
12 M. Brinkmann, P. Turek, J.-J. Andre, *J. Mater. Chem.,* 1998, **8**, 675-685.
13 G. Ilangovan, J. L. Zweier, P. Kuppusamy, *J. Phys. Chem. B,* 2000, **104**, 9404-9410.
14 P. Turek, J.-J. Andre, A. Giraudeau, *Chem. Phys. Lett*., 1987, **134**, 471-476.
15 P. Turek, M. Moussavi, P. Petit, J.-J. Andre, *Synth. Met.,* 1989, **29**, F65-F70.
16 F. Bensebaa, J.-J. Andre, *J. Phys. Chem.,* 1992, **96**, 5739-5745.
17 P. E. Fielding, F. Gutman, *J. Chem. Phys.*, 1957, **26**, 411-419.
18 K. Yakushi, T. Ida, A. Ugawa, H. Yamakado, H. Ishii, H. Kuroda, *J. Phys. Chem.*, 1991, **95**, 7636-7641.
19 M. Inagawa, H. Yoshikawa, T. Yokoyama, K. Awaga, *Chem. Commun.*, 2009, 3389-3391.
20 J. M. Green, L. R. Faulkner, *J. Am. Chem. Soc.*, 1983, **105**, 2950-2955.
21 H. Homborg, C. L. Teske, *Z Anorg. Allg. Chem.,* 1985, **527**, 45-61.
22 G. M. Sheldrick, SHELXS-97: Program for crystal structure solution, University of Göttingen (Germany), 1997.
23 G. M. Sheldrick, SHELXL-97: Program for crystal structure refinement, University of Göttingen (Germany), 1997.
24 G. Ilangovan, J. L. Zweier, P. Kuppusamy, *J. Phys. Chem. B,* 2000, **104**, 4047-4059.
25 K. Sakthivel, N. Munichandraiah, L. G. Scanlon, *J. Electrochem. Soc.,* 2005, **152**, C756-C763.
26 T. Laaksonen, V. Ruiz, L. Mutomäki, B. M. Quinn, *J. Am. Chem. Soc.*, 2007, **129**, 7732-7733.
27 *Electrochemical Methods: Fundamentals and Applications*, A. J. Bard and L. R. Faulkner, Wiley, New York, 2001.
28 CCDC 979678 (for LiPc), 979679 (for $LiPcCl_{0.11}$), 979680 (for $LiPcCl_{0.20}$), 979681 (for $LiPcCl_{0.21}$), 979682 (for $LiPcCl_{0.24}$), 979683 (for $LiPcCl_{0.38}$), and 996929 (for $LiPcCl_{0.46}$) contain the supplementary crystallographic data for this paper. These data can be obtained free of charge via www. ccdc.cam.ac.uk/conts/retrieving.html (or from the Cambridge Crystallographic Data Centre, 12 Union Road, Cambridge CB21EZ, U.K.; fax (+44)1223-336-033 or e-maildeposit@ccdc.cam.ac.uk).
29 B. N. Diel, T. Inabe, J. W. Lyding, K. F. Schoch, Jr., C. R. Kannewurf, T. J. Marks, *J. Am. Chem. Soc.*, 1983, **105**, 1551-1567.
30 P. Petit, P. Turek, J.-J. Andre, R. Even, J. Simon, R. Madru, M. A. Sadoun, G. Guillaud, M. Maitrot, *Synth. Met.*, 1989, **29**, F59-F64.
31 M. Dumm, P. Lunkenheimer, A. Loidl, B. Assmann, H. Homborg, P. Fulde, *J. Phys. Chem*., 1996, **104**, 5048-5053.

Graphical Abstract

Solid-state electrochemical doping of Cl^- ions to nanoporous LiPc crystals induces crystal-to-crystal transformation to LiPc·Cl_x, suggesting a strong electron correlation in a 1D half-filled electron system of LiPc.